Available online at www.sciencedirect.com

SciVerse ScienceDirect

Ceramics International 38 (2012) 5731–5740

CERAMICS INTERNATIONAL

www.elsevier.com/locate/ceramint

Synthesis and characterization of CuO-hybrid silica nanocomposite coatings on SS 304

R. Subasri *, R. Malathi, A. Jyothirmayi, N.Y. Hebalkar

International Advanced Research Centre for Powder Metallurgy and New Materials (ARCI), Balapur, Hyderabad 500005, Andhra Pradesh, India

Received 7 February 2012; received in revised form 16 March 2012; accepted 5 April 2012
Available online 13 April 2012

Abstract

Pure and CuO-dispersed hybrid silica nanocomposite coatings were generated using sols synthesized from acid catalyzed hydrolysis and condensation of n-propyl trimethoxysilane and tetraethoxysilane in combination with copper nitrate. Coatings were initially deposited on soda lime glass substrates by dip coating followed by heat treatment at 150, 250 and 350 °C for 2 h in air and characterized. Coatings were subsequently deposited by dip coating on stainless steel 304 substrates. An optimized heat treatment temperature of 250 °C was chosen based on the contact angles of coatings on soda lime glass substrates and results of thermogravimetric/differential thermal analysis on the dried gels obtained from the sol synthesized from the combination of n-propyl trimethoxysilane and tetraethoxysilane. Gels heat-treated at 250 °C were characterized by X-ray diffraction, X-ray photoelectron spectroscopy and transmission electron microscopy for crystallinity. Characterization of the coatings was carried out with respect to thickness, water contact angle and adhesion. Corrosion testing of coatings on SS 304 was studied by potentiodynamic polarization measurements and electrochemical impedance spectroscopy after 1 h and 24 h exposure to 3.5% NaCl. The corrosion resistances of CuO-dispersed hybrid silica coatings after 1 h and 24 h exposure to 3.5% NaCl solution were higher than that of pure hybrid silica coatings, both of which had thicknesses ranging from 140 nm–200 nm.

Keywords: A. Sol–gel processes; A. Films; B. Nanocomposites; C. Corrosion; E. Biomedical applications; $CuO–SiO_2$

1. Introduction

The sol–gel process has excellent potential for generation of purely inorganic or organic–inorganic hybrid coatings. In case of the latter, where one can incorporate an organic component into the inorganic network, the process opens up a wide range of possibilities for multi-functionalizing and tailoring of the coating. Through modification of the chemical composition of the starting materials, the introduction of multi-functionalities such as anti-bacterial property, hydrophobicity, improved mechanical strength etc. can be realized in a single layered coating. Usually, sol–gel derived coatings possessing multi-functionalities like anti-bacterial, hydrophobicity and corrosion resistance, when intended for applications on surgical equipment, make use of anti-bacterial Ag nanoparticles dispersed in sols that yield hydrophobic or low surface-free-energy coatings [1–4]. Due to the increasing concerns on the toxicity of Ag nanoparticles when used for anti-bacterial applications [5], it becomes highly relevant to look for alternate anti-bacterial materials that can be dispersed in hybrid sols to generate anti-bacterial coatings. However, reports on use of non-silver antibacterial nanoparticles like CuO for generating the coatings are scarce, though the anti-bacterial properties of CuO are well-known in the literature [6–9]. Perelshtein et al. [6] have tested the anti-bacterial activities of CuO-fabric nanocomposite using *Escherichia Coli* (Gram negative) and *Staphylococcus Aureus* (Gram positive) and found a considerable amount of anti-bacterial activity by using a low concentration of 1–1.5 wt % CuO. Very recently, Akhavan and Ghaderi [9] have reported on their investigation of Cu and CuO nanoparticles immobilized by purely inorganic silica films for antibacterial applications.

As regards synthesis of hydrophobic coatings using sol–gel process, these are commonly generated by hydrolysis and condensation of alkyl modified alkoxy silanes or fluorosilanes. However, since fluorinated materials like fluorosilanes are not environment friendly, alkyl modified alkoxy silanes are preferred for generation of hydrophobic coatings.

* Corresponding author. Tel.: +91 40 24443567; fax: +91 40 24442699.
E-mail address: subasri@arci.res.in (R. Subasri).

0272-8842/$36.00
http://dx.doi.org/10.1016/j.ceramint.2012.04.018

Therefore, in order to generate an eco-friendly, hydrophobic, anti-bacterial surface that is non-fluorinated and which contains a non-silver anti-bacterial agent, CuO nanoparticles could be dispersed in a hydrophobic sol–gel matrix derived from hydrolysis and condensation of an alkyl modified alkoxy silane. Keeping in view of a potential application of use of such nanocomposite coatings for surgical equipment made of stainless steel (such as SS 304 or 316), corrosion resistance of the coating would also be of great concern.

There have been only few reports on synthesis and characterization of CuO–inorganic SiO_2 and CuO–TiO_2 sol–gel nanocomposite coatings for specific applications like improving corrosion resistance of Al alloys and for photocatalytic, anti-microbial activity [10,11] respectively. Though various organic coatings [12–14], pure inorganic [15,16] as well as organic–inorganic hybrid coatings by sol–gel processing [17–23] have been studied for corrosion protection of stainless steel 304, there are no reports on use of CuO-based sol–gel coatings on SS 304.

Hence, the objective of the present investigation was to synthesize and characterize CuO-hybrid silica coatings with more focus on their corrosion resistance properties as a preliminary investigation prior to their potential use as multifunctional (i.e., anti-bacterial, hydrophobic and corrosion resistant) coatings for surgical equipment.

Pure and CuO-dispersed organic–inorganic hybrid silica coatings on SS 304 substrates were derived from n-propyl trimethoxysilane and tetraethoxysilane in combination with copper nitrate and were investigated for their adhesion, thickness, water contact angles, and corrosion resistance in 3.5% NaCl solution.

2. Experimental

2.1. Materials

Tetraethoxysilane (abbreviated as TEOS, ABCR, Germany, 97%), n-propyl trimethoxysilane (abbreviated as nPTMOS, Gelest, Inc., USA, 97%), Copper nitrate, Hydrochloric acid (AR grade) and ethanol were used as starting materials. Coatings were generated on Soda lime glass (SLG) substrates of dimensions 75 mm × 25 mm × 1 mm as well as on stainless steel 304 substrates of dimensions 100 mm × 100 mm × 1 mm with a matt finish surface. The SLG substrates were cleaned using 15 vol% solution of a commercial cleaning agent INDROX® followed by thorough rinsing using de-ionized water. The final rinsing was carried out using isopropanol and the SLG substrates were used immediately after cleaning for coating deposition. The as-supplied SS 304 substrates had a protective adhesive tape to prevent formation of scratches during handling. After removal of the protective tape, they were thoroughly degreased with acetone prior to coating.

2.2. Sol synthesis

Organic–inorganic hybrid silica sols were synthesized by hydrolysis and polycondensation of ethanol diluted TEOS in presence of HCl as a catalyst and nPTMOS as a co-precursor at room temperature. Initially, various compositions with mole-ratios of TEOS and nPTMOS varying from 1:0 to 0:1 was used for synthesizing the matrix sol. The TEOS and nPTMOS mixture was diluted with ethanol by vigorous stirring. This was hydrolyzed with deionized water using HCl as the catalyst and stirred for 3 h at 23 °C. The optimum composition yielding maximum hydrophobicity was chosen as the matrix sol for making the CuO-hybrid silica composite sol. To the optimized hybrid silica sol composition, 10 mol% of copper nitrate that was pre-diluted with ethanol was added under vigorous stirring. This mixture was then hydrolyzed with deionized water using HCl as the catalyst and stirred for 3 h at 23 °C. The plain and CuO-hybrid SiO_2 sols were filtered with 0.4 μm pore size membrane filter and used for coating.

2.3. Coating deposition

Coatings were generated by dip coating technique initially on SLG substrates for optimization of the TEOS-nPTMOS composition and heat treatment temperature. Based on maximum hydrophobicity obtained, the coatings were thermally cured in air at 250 °C for 2 h with a ramp rate of 1 K/min for densification. Subsequently, coatings were obtained on stainless steel 304 substrates using the optimized hybrid silica sol and CuO–SiO_2 sol composition by dip coating using withdrawal speeds of 1 mm/s, 3 mm/s, 5 mm/s and 7 mm/s. Coatings on SS were densified using same heating schedule as optimized for the SLG substrates, i.e., at 250 °C for 2 h. Henceforth, the coatings derived from the optimized hybrid silica sol and copper oxide-hybrid silica sols will be abbreviated as S and CS respectively.

2.4. Characterization

5 ml of the hybrid silica sol with different compositions was dried and thermogravimetric/differential thermal analysis (TG/DTA) measurements were carried out on the dried gel using a Netzsch Simultaneous Thermal Analyzer. The nPTMOS:TEOS ratio and heat treatment temperature for coatings was optimized based on results of TG/DTA. The crystallinity of the CuO–SiO_2 composite system was verified by using XRD and XPS analysis. XRD analysis was carried out using a Brukers D8 Advance X-ray diffractometer (XRD) employing Cu $K\alpha_1$ radiation. XPS analysis was carried out using an Omicron Nanotechnology, UK (model ESCA+) X-ray Photoelectron spectrometer. The crystallite size of the copper oxide was determined using transmission electron microscope (TEM, Technai 200 G2, FEI, Netherlands). A drop of the dispersion of powdered CS gel in 5 ml of ethanol was dispensed on a polymer coated copper grid and used for TEM analysis.

The coated SS substrates were inspected by optical and scanning electron microscope (Hitachi S-4300SE/N equipped with a field emission gun) for microstructure and presence of defects, if any. Coating thickness was measured using a spectroscopic ellipsometer (J.A. Woollam, USA). Water contact angle was measured by a Krüss GmbH, Germany,

drop shape analyzer DSA 100, to verify the hydrophobicity/hydrophilicity of the coatings. Adhesion of the coatings to the substrate was measured by tape test using a cross hatch cutter, according to ASTM D3359-02.

2.5. Corrosion testing

The coated surfaces of SS 304 substrates were exposed for 1 h and 24 h to a 3.5% NaCl solution purged with N_2 gas. Polarization and impedance data were collected at 25 °C using a computer controlled Solartron Electrochemical interface (Model SI 1287) and frequency response analyzer (Model SI 1260). The corrosion test cell had the classic configuration of three electrodes (platinum as counter-electrode, a saturated calomel electrode as a reference electrode and coated metallic sample as working electrode). Potentiodynamic scan was performed from cathodic to anodic region from −0.6 to 0.4 V with a scan rate of 1 mV/s. The electrochemical impedance scan was carried out using an AC signal of 10 mV amplitude applied over a bandwidth from 100 kHz to 0.03 Hz. Five dip coated samples, i.e., 10 coated surfaces, for each set were used for corrosion testing to ascertain the reproducibility of the data. The results obtained were analyzed using CORRVIEW2 and ZVIEW2 software and compared with those obtained for bare substrate.

3. Results and discussion

3.1. Characterization

The water contact angles of the coatings on soda lime glass substrates generated by employing different withdrawal speeds for varying mole ratios of nPTMOS:TEOS and heat treated at different temperatures are shown in Table 1. It can be seen from Table 1 that at any temperature below 350 °C, the contact angles increased with the increase in the concentration of nPTMOS up to a composition of 3:1 nPTMOS:TEOS. Coatings generated from only TEOS are usually hydrophilic (or less hydrophobic) due to presence of large number of Si–OH groups that are generated by the complete hydrolysis of the ethoxy groups. When nPTMOS is co-hydrolyzed with TEOS, it is expected that the replacement of one of the methoxy groups in tetramethoxysilane (TMOS) by the non-hydrolyzable n-propyl ($–C_3H_7$) group present in nPTMOS would result in higher hydrophobicity of coatings due to the surface reorientation of the n-propyl organic group. When mole ratios of nPTMOS:-TEOS in the sol increases, the water contact angles of the coatings generated from these sols also increase due to higher concentration of n-propyl groups on the surface. Accordingly, it can be seen from Table 1 that coatings from pure nPTMOS showed the highest hydrophobicity only at 150 °C. However, pure nPTMOS was not considered as an optimized composition based on hydrophobicity, since hybrid coatings are usually synthesized by co-hydrolyzing an alkyl modified silane along with a tetraalkoxy silane, so as to get good mechanical properties. Hence, coatings from pure nPTMOS were not considered for the corrosion studies since they are not expected to possess good mechanical properties. The composition of 3:1 nPTMOS:TEOS was optimized as the matrix sol composition since it exhibited maximum hydrophobicity when compared to other compositions.

In order to optimize the heat treatment temperature, the water contact angles measured at different temperatures were compared. The hydrophobic hybrid silica films were found to retain their hydrophobicities up to a temperature of ∼250 °C and above this temperature, the coatings became hydrophilic, as seen from the water contact angles measured at 350 °C. This is due to the fact that, at this temperature, the n-propyl groups on the surface get oxidized into –Si–OH groups, which are known to be hydrophilic. Since the objective of the present study was to investigate on the applicability of the multi-functional coatings, i.e., corrosion resistant, hydrophobic, anti-bacterial, for surgical equipment, the composition and heat treatment temperature had to be optimized so as to achieve maximum hydrophobicity along with good barrier and mechanical properties, which is achieved by higher densification. Hence, though one could still obtain a hydrophobic coating at 150 °C, the optimized heat treatment temperature for the coatings was fixed at 250 °C, where the coatings could be expected to have densified sufficiently as well as retained the hydrophobicity.

The observations made from the water contact angle data measured as a function of temperature matched well with inferences from TG/DTA measurements as shown in Fig. 1. There is a mass loss occurring around 100 °C due to loss of water and another large one occurring at different temperatures for different compositions. In case of the 3:1 ratio of nPTMOS:TEOS, the mass loss starts from ∼350 °C and shifts to higher temperatures for increasing TEOS content. The

Table 1
Contact angles for different compositions of nPTMOS/TEOS coatings generated using different withdrawal speeds (mm/s) on soda lime glass substrates and heat treated at different temperatures.

Composition	Water contact angles [degrees]					
	150 °C		250 °C		350 °C	
nPTMOS:TEOS	1 mm/s	2 mm/s	1 mm/s	2 mm/s	1 mm/s	2 mm/s
0:100	81 ± 3	80 ± 4	31 ± 2	31 ± 5	12 ± 4	11 ± 2
25:75	88 ± 3	88 ± 3	87 ± 2	88 ± 1	22 ± 6	20 ± 7
50:50	92 ± 6	92 ± 4	92 ± 3	91 ± 2	25 ± 5	24 ± 3
75:25	97 ± 6	96 ± 2	91 ± 3	94 ± 4	41 ± 8	48 ± 2
100:0	102 ± 5	103 ± 3	86 ± 2	84 ± 3	9 ± 5	8 ± 2

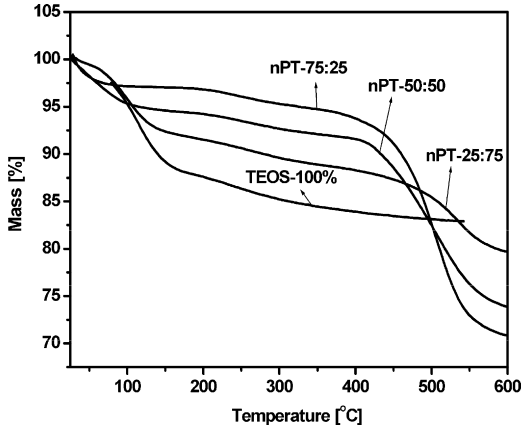

Fig. 1. Results of the thermogravimetric analysis on dried gels of different compositions of n-propyl trimethoxy silane (nPTMOS) and tetraethoxy silane (TEOS).

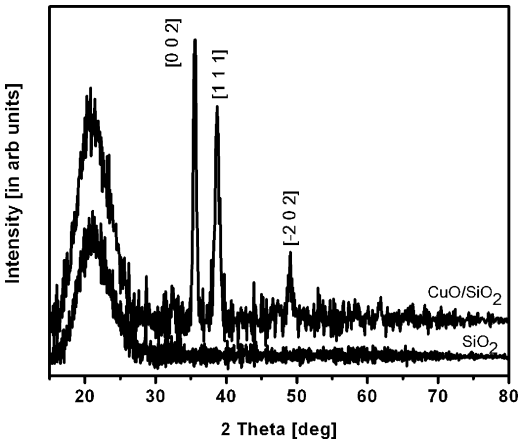

Fig. 2. XRD patterns for SiO_2 and CuO/SiO_2 gels heat treated at 250 °C for 2 h.

magnitude of mass loss increases with increasing concentration of the organically modified silane in the hybrid silica sol (17.5%, 20.5%, 25.8% and 29.3% for nPTMOS:TEOS varying from 0:1 to 3:1).

From TG/DTA measurements on the dried gels and water contact angle measurements on the coatings deposited on soda lime glass substrates, the composition of the hybrid sol was optimized to be 75:25 nPTMOS:TEOS and heat treatment temperature as 250 °C for 2 h. This optimized composition was used for synthesizing $CuO–SiO_2$ sol for subsequent coatings on SS substrates.

The XRD pattern of the heat treated gels S and CS at 250 °C for 2 h is shown in Fig. 2. The XRD pattern of S shows only a huge broad hump characteristic of amorphous silica network, whereas that of CS shows crystallinity along with the broad hump. The first three intense peaks occurring at 2θ values of 35.56°, 38.64° and 48.9° in the XRD pattern of CS, corresponding to orientations along the crystallographic planes

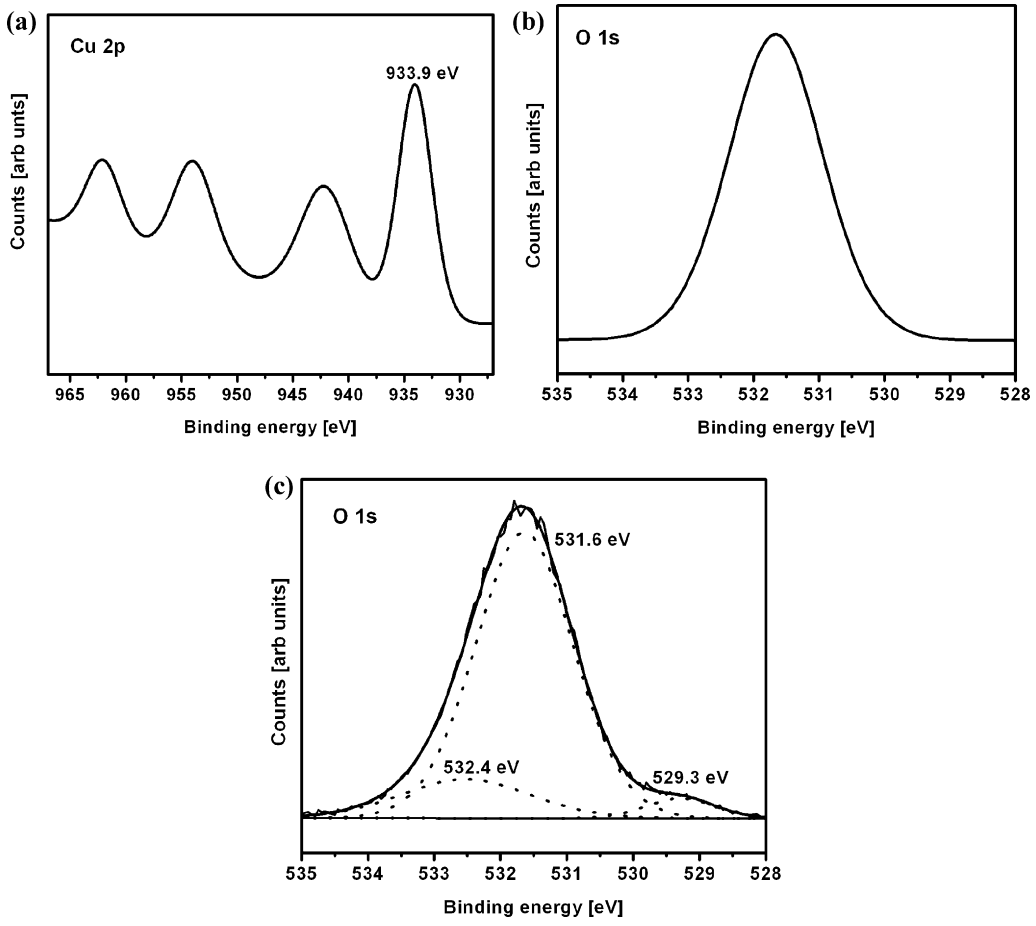

Fig. 3. XPS narrow spectra of heat treated gels of (a) Cu 2p in copper-hybrid silica; (b) O 1s spectrum in hybrid silica and c) O 1s spectrum in copper-hybrid silica.

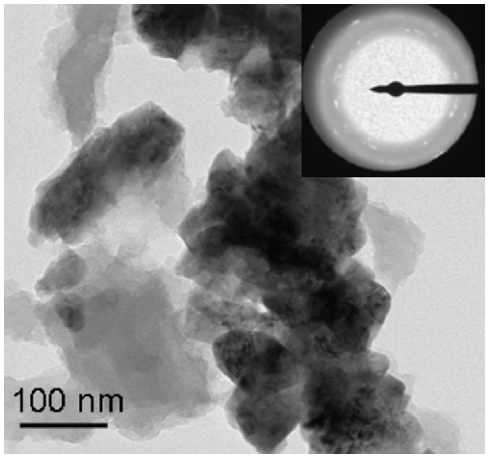

Fig. 4. Bright field image of the heat treated CS gel (inset shows the selected area diffraction pattern).

[0 0 2], [1 1 1] and [−2 0 2], respectively are the characteristic peaks of copper oxide (JCPDS card no. 45-0937) which was crystallized in an amorphous silica network. XPS spectrum also showed presence of copper in its oxide form in copper-hybrid silica sample after heat treatment at 250 °C, as depicted in Fig. 3. O 1s has a single peak in hybrid silica which appeared at 531.6 eV. However, when copper oxide was introduced in the hybrid silica matrix, three components in the O 1s peak were observed which were at 531. 6, 529.3 and 532.5 eV as shown in Fig. 3b and c respectively. The first component is as that of oxygen in hybrid silica. The additional two components can be attributed to the copper oxide in the silica matrix. The TEM image as shown in Fig. 4 showed the presence of nanocrystalline material dispersed in an amorphous matrix. The sizes of the crystallites were seen to vary from 60 to 70 nm. The electron diffraction (ED) image shown as an inset in Fig. 4 also confirmed the crystallinity of the particles seen in the image. Since it was already confirmed that only CuO and not silica had crystallized from XRD studies, the phase that showed crystallinity in TEM ED analysis was attributed to CuO coming from the sample.

The thickness of S and CS coatings on SS ranged from 140 nm–200 nm. A typical ellipsometric data for the S coating is shown in Fig. 5a. The thickness of coatings obtained in the present study matched well with similar type of hybrid silica coatings obtained in Refs. [17–19] using similar withdrawal speeds. The water contact angles for S coatings for different withdrawal speeds varied from 80° to 87° and those for the CS coatings ranged from 83° to 95°, representative images are shown in Fig. 5b and c. The difference in water contact angles obtained for the same silica coatings on soda lime glass and SS substrates can be attributed to the difference in the surface finish of substrates. The roughness of the SS substrate was measured to be ∼0.3 μm and that of SLG was <0.01 μm. Since SLG has surface –Si–OH (silanol) groups, adhesion of silane based sol–gel coatings on glass is usually very high. Hence,

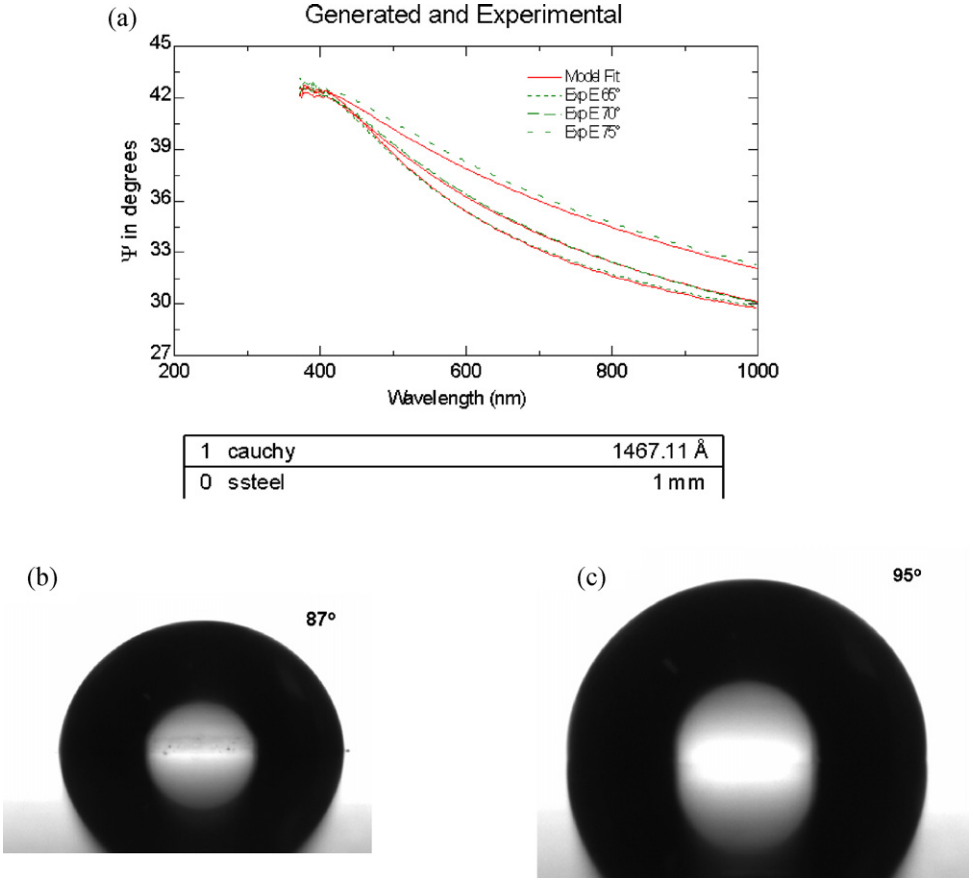

Fig. 5. Results of characterization of coatings on SS 304 (a) ellipsometric data for S-, (b) water contact angle of S-7 and (c) water contact angle of CS-7.

adhesion testing was carried out only on SS and could be graded with the classification of 5B (0% peeling off) as observed under optical microscope after adhesion testing, which implies very good adhesion to the substrate surface.

3.2. Corrosion tests

3.2.1. Electrochemical polarization studies

Potentiodynamic polarization measurements were carried out on coatings generated using S and CS sols using different withdrawal speeds of 1 mm/s, 3 mm/s, 5 mm/s and 7 mm/s to investigate on the effect of coating thickness on corrosion resistance. The coating thickness normally depends on withdrawal speed according to Landau–Levich equation [24], if the sol is a Newtonian fluid. The equation however, does not take into account, effect of surface roughness on coating thickness. In the present investigation, due to low viscosity of sol and due to the matt finish of the substrate surface, the coatings deposited with varying withdrawal speeds do not show significant difference in thickness, which values are comparable to the scatter in the thickness values. However, the effect of withdrawal speed (variation in coating thickness) can be realized from the sensitive electrochemical polarization or impedance measurements. The polarization curves of SS 304 substrates coated with S and CS coatings using different withdrawal speeds after 1 h exposure to 3.5% NaCl are shown in Fig. 6a and b and for S and CS coatings deposited with 1 mm/s withdrawal speed after 1 h and 24 h exposure to 3.5% NaCl are shown in Fig. 6c and d. In case of S coatings, S-3, S-5 and S-7 show corrosion potentials lower than that of the bare SS 304. The same observation, i.e., E_{corr} of coated SS 304 being lower than bare SS 304 has already been reported for organic–inorganic hybrid silica coatings derived from tetraethoxysilane and methacryloxypropyltrimethoxy silane [Refs. 17–19]. The authors in Refs. [17–19] attributed the reduction in open circuit potential to the effective suppression of the cathodic reaction due the reason that SiO_2 having a low isoelectric point (1.7–3.5) leads to a negative surface charge at pH >2. Alternately, in the case of CS coatings, only for the coatings with higher withdrawal speeds 5 and 7 mm/s, the corrosion potential is lower than the bare 304 SS, which is slightly higher than that for an S coating with same withdrawal speed. In case of 1 and 3 mm/s, the E_{corr} values for CS coatings are nearly the same as that of bare 304 SS. Since the isoelectric point of CuO is 9.5 and that for SiO_2 is between 1.7 and 3.5, a mixed effect is observed for the CuO-hybrid silica nanocomposite coating when immersed in a 3.5% NaCl solution, which has a pH of 6.5–7 and hence, the E_{corr} of a thicker CuO-silica coating is more positive than for a pure hybrid silica coating generated using the same withdrawal speed.The protective behavior of coatings is however similar in both the types of coatings but the protective region, i.e., the passive potential range is increased more in case of samples coated with CS for example the ΔE is 520 mV when compared to 250 mV for S coated sample with 7 mm/s withdrawal speed and near to that of bare substrate with 550 mV. R_p fitting of the polarization data yielded the different

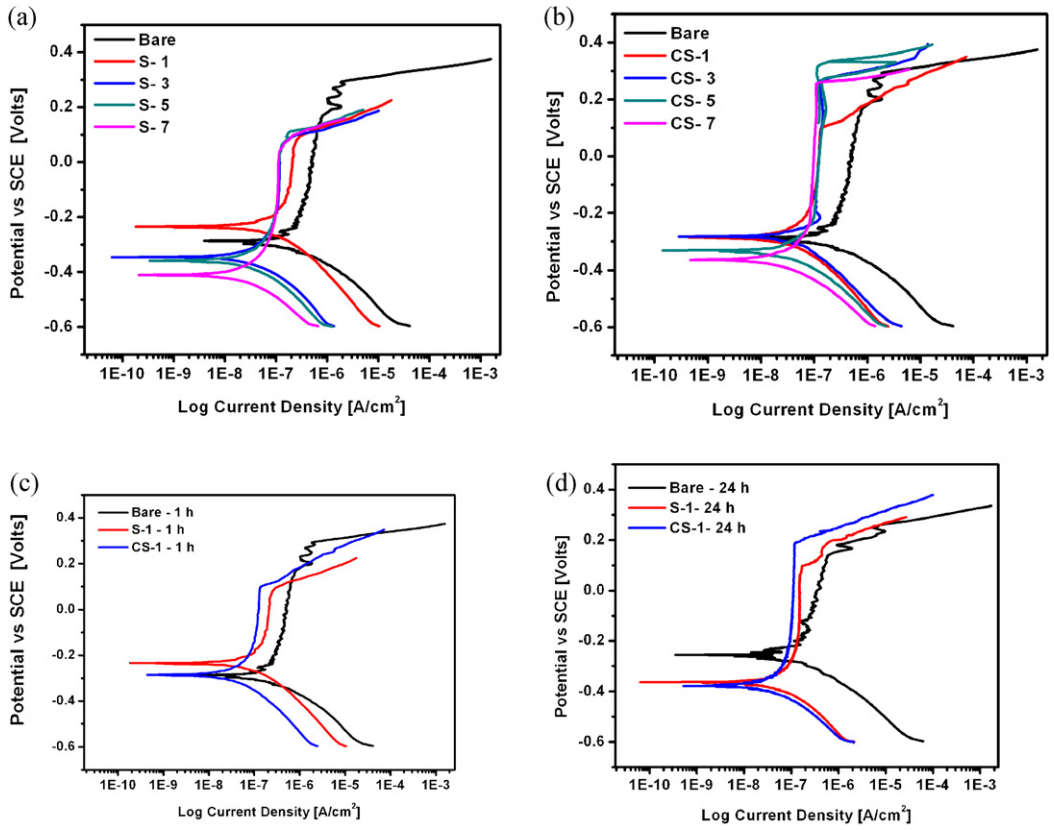

Fig. 6. Comparison of polarization data obtained for (a) S and (b) CS coatings generated using different withdrawal speeds 1, 3, 5, 7 mm/s (labeled as S-1 to S-7 and CS-1 to CS-7 respectively) and for S-1 and CS-1 coatings for (c) 1 h and (d) 24 h exposure to 3.5% NaCl.

Table 2
Results obtained from the R_p fitting of the polarization data shown in Fig 6a–d for 1 h and 24 h exposure to 3.5% NaCl at 25 °C.

Samples-coating withdrawal speed (mm/s)	Exposure time (h)	Corrosion potential, E_0 (V)	Corrosion current density, I_{corr} (E^{-8} A/cm^2)	Polarization resistance, R_P (E^5 Ω cm^2)	Protection efficiency (%)
Bare SS 304	1	−0.289	17.09	1.53	–
S-1	1	−0.234	6.68	3.90	60
S-3	1	−0.344	2.94	8.85	83
S-5	1	−0.358	2.76	9.47	84
S-7	1	−0.409	2.32	11.24	86
CS-1	1	−0.285	3.08	8.48	82
CS-3	1	−0.282	4.67	5.59	73
CS-5	1	−0.334	3.25	8.04	81
CS-7	1	−0.363	2.42	10.78	86
Bare SS 304	24	−0.258	9.46	2.76	–
S-1	24	−0.365	4.73	5.52	50
CS-1	24	−0.376	3.31	7.88	65

electrochemical parameters like corrosion current density, corrosion potential, polarization resistance and protection efficiencies, which are summarized in Table 2. As can be seen from Table 2, all the coated surfaces improved greatly the corrosion resistance of SS 304 and had indeed provided a physical barrier to block the electrochemical processes. The corrosion current density of a CS coating generated using a withdrawal speed of 1 mm/s is almost the same value as that of a substrate with S coating generated at a higher withdrawal speed of 3 mm/s (i.e., coating with higher thickness). Hence, it could be seen that the substrate with CS coatings provide better corrosion protection even at a minimum withdrawal speed of 1 mm/s, when compared to S coatings on the substrate generated using the same withdrawal speed. In case of S coatings, the corrosion current density had progressively decreased with increasing withdrawal speed (increasing thickness), which again is indicative of a better barrier protection with thicker coatings as also observed in Ref. [17] where thick hybrid silica coating generated by depositing 2 layers was found to increase the corrosion resistance of SS 304 than a single layer coating. In case of CS coatings, however, no trend was observed with respect to corrosion density versus withdrawal speed. The protection efficiencies of the coatings were calculated from the polarization data using the formula,

$$\text{Protection efficiency, PE } (\%) = \left(\frac{1 - i_{corr}}{i^{\circ}_{corr}}\right) \times 100 \qquad (1)$$

where i_{corr} and i°_{corr} are the corrosion current densities of the coatings and bare substrate respectively. The protection efficiencies of S coatings are seen to increase with increasing coating thickness, which were generated by increasing the withdrawal speeds. In case of CS coatings, starting from a thin coating (generated using a withdrawal speed of 1 mm/s), the protection efficiency is always high and not significantly different from each other except that measured for that generated using a withdrawal speed of 3 mm/s, the reason for which is not clear at this stage. At very high withdrawal speeds, the S and CS coatings exhibit equal protection efficiencies. The important point to be noted is that a CS coating generated at low withdrawal speeds of 1 mm/s with thickness ~140–150 nm is still able to provide higher protection efficiency than an S coating generated at the same withdrawal speed that has a similar thickness, reason for which could be due to covering of defects/porosities in the coatings by the nanocrystalline CuO dispersed in the hybrid silica matrix. The CS coatings provide better corrosion protection than S coatings for 1 h and 24 h exposure to 3.5% NaCl solution.

3.2.2. Electrochemical impedance spectroscopy

The S and CS coatings on SS 304 were also evaluated by electrochemical impedance spectroscopy (EIS) in order to gain more insight into their barrier properties and adhesion to the substrate by exposure to 3.5% NaCl for 1 h and 24 h. The impedance spectra obtained for the S and CS coatings for 1 h

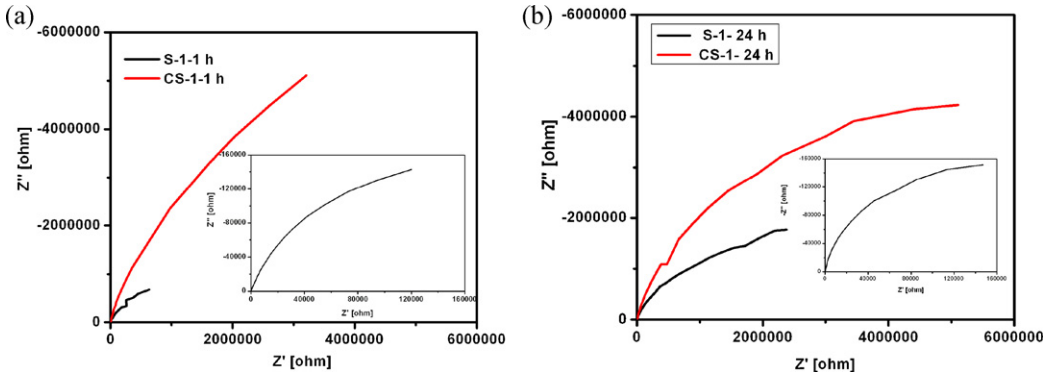

Fig. 7. Nyquist plots for S and CS coatings for (a) 1 h and (b) 24 h exposure to 3.5% NaCl solution with insets showing the Nyquist plots for the bare substrate.

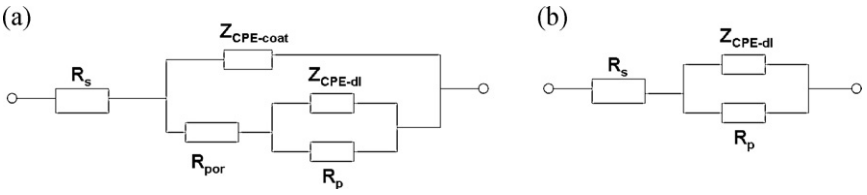

Fig. 8. Models of equivalent circuits used to fit the obtained impedance data of (a) S coated substrate and (b) bare and CS coated substrate.

and 24 h exposure are displayed as Nyquist plots in Fig. 7a and b respectively. Fig. 8a represents the equivalent circuit that was used to model the substrate coated using S and Fig. 8b to model the substrate coated using CS and the bare substrate. A constant phase element (CPE) was used instead of an ''ideal capacitor'' to explain the deviations from ideal behavior. The possible reasons for a non-ideal behavior could be due to surface roughness, inhomogeneous reaction rates on the surface, or varying thickness or composition of a coating [25–27]. The impedance of a CPE, i.e., Z_{CPE} could be defined as $Z_{CPE} = 1/Y(j\omega)^n$, where ω is the angular frequency in rad s^{-1}, Y is the pseudo-capacitance and n is called the CPE exponent, which is associated with the system inhomogeneity. When $n = 1$, the system behaves like a pure capacitor and $Y = C$. When CPE is used to fit the experimental data, $n < 1$, R_s is the resistance of the electrolyte, R_{pore} is the pore resistance of the coating, Y_{coat} is the pseudo-capacitance associated with the double layer formed at the metal–electrolyte interface. Table 3 presents the fitting parameters for the bare substrate and coated samples exposed to 3.5% NaCl for 1 h and 24 h obtained from the impedance data using the equivalent circuits as shown in Fig. 8. Two time constants are obtained for samples coated with S for both 1 h and 24 h exposure time. The time constant at high frequencies is related to the properties of coating. Since the sol–gel coatings act as dielectric material the corrosion might have occurred due to penetration of electrolyte through defects and pores. The R_{pore} has been introduced in the first time constant, which shows the resistance of the solution in the pores. The pore resistance 47.0 Ω cm^2 for 1 h, which is very less, shows the presence of more porosity in the coating. The R_{pore} value is seen to have increased after 24 h exposure due to blocking of the pores by the corrosion product, as a result of which, the R_p value also is increased. In case of CS coatings, a single time constant is obtained showing the lowest porosity and, the R_p value is very high for CS when compared to that of S coatings. From the R_p values in Table 3 and from the Nyquist plots (Fig. 7), it can be seen that coated substrates offered higher resistance to corrosion when compared to the bare substrate, be it S or CS coatings; a higher R_p value implies higher corrosion resistance. This shows the promising barrier properties of both S and CS coatings on SS 304. Even after 24 h of exposure to 3.5% NaCl, CS coatings are better than S coatings having similar thicknesses of 140–150 nm. The time of 24 h is not sufficient to reveal any porosity in the coating which could lead to coating degradation. The possible reasons for the improved corrosion resistance of CS coatings when compared to S coatings are discussed below.

A sol derived from higher content of the organically modified silane, i.e., nPTMOS (75 mol%) in combination with TEOS, i.e., coating S, was seen to exhibit water contact angles as high as 87°, which had further slightly increased to 95° for the CS nanocomposite coating. The improved hydrophobicity in the CS coating could possibly be due to the presence of copper oxide nanoparticles, which has created some amount of nanoscaled roughness on the surface, leading to increased water contact angles. It is well documented in the literature that a textured surface can lead to reduction in contact area of any component, e.g., water to the surface [28]. A textured surface is a surface which is not smooth within a small observed area, but has elevations or small amount of roughness, which leads to improved water repellent properties. The textures may be in the form of whiskers or nanoparticles protruding from the surface. The two main well-known models that attempt to explain the improved hydrophobicity due to topography and roughness were given by Wenzel [29] and Cassie–Baxter [30]. For example, in case of a Wenzel surface state, the apparent contact angle can be given by the equation given below:

$$\cos\theta* = r\cos\theta \quad (2)$$

where θ^* is the apparent contact angle, r is the roughness and θ is the contact angle of an ideal smooth surface. Here, the liquid fills the roughness grooves of the surface. Thus, as the roughness increases, the contact angle will increase, reflecting an increase in the relative hydrophobicity.

This aspect could be one reason for the higher corrosion resistance of a CS coating, when compared to S coating generated using the same withdrawal speed of 1 mm/s, since a higher hydrophobicity means more water repellence and lesser

Table 3
Fitting parameters obtained using the impedance data presented in Fig. 7 and equivalent circuits shown in Fig. 8.

Sample	R_s (Ω cm^2)	C_{coat} (Ss^n cm^{-2})	R_{pore} (Ω cm^2)	n_{dl}	C_{dl} (Ss^n cm^{-2})	R_p (Ω cm^2)	χ^2
Bare SS-1 h	2.583	–	–	0.859	4.646E−5	4.041E5	0.004
S-1 mm/s-1 h	14.27	9.406E−7	47.08	1	7.012E−6	1.463E6	0.014
CS-1 mm/s-1 h	29.75	–	–	0.881	6.96E−7	1.443E7	0.005
Bare SS-24 h	3.571	–	–	0.929	4.675E−5	3.465E5	0.011
S-1 mm/s-24 h	12.31	1.266E−6	3.138E6	0.819	7.712E−6	2.842E6	0.002
CS-1 mm/s-24 h	41.71	–	–	0.854	1.071E−6	1.053E7	0.01

wetting of the electrolyte which in turn implies higher corrosion resistance.

The other reason for higher corrosion resistance of CS coatings could be due to presence of nanocrystalline CuO dispersed in the hybrid silica matrix. Organic–inorganic hybrid coatings are known to be porous because of lower networking due to presence of the non-hydrolyzable organic groups. The CuO nanocrystallites could help in filling the porosity in the hybrid silica matrix for which the pore size could be of the order of 60–70 nm that matches well with that of the CuO crystallite sizes. A decreased porosity in the coating implies a better barrier protection of the substrate against the electrolyte. This could be a contributing factor for the increased corrosion resistance of even 140–150 nm thick CS coatings.

The present study showed the promise of organic–inorganic hybrid nanocomposite multifunctional coatings for improving the corrosion resistance of SS 304.

4. Conclusion

Hybrid organic–inorganic silica and copper oxide-hybrid silica nanocomposite coatings based on n-propyl trimethoxy silane and tetraethoxy silane have been investigated for corrosion protection of SS 304. Both pure hybrid silica and copper oxide-hybrid silica nanocomposite coatings provided a very good barrier type protection and improved the corrosion resistance of the SS 304 substrate. Copper oxide-silica nanocomposite coatings having thicknesses ranging from 140 to 200 nm were found to increase the corrosion resistance of SS 304, when compared to pure hybrid silica coatings of even thicknesses. Presence of nanocrystalline CuO imparts a nanoscaled roughness that further increases the water contact angle that contributes to improved corrosion resistance of the CuO-hybrid silica nanocomposite coatings when compared to hybrid silica coatings. The present investigation proved the promise of CuO-hybrid silica nanocomposite coatings for improving the corrosion resistance of SS 304. Further investigations are underway to test the anti-bacterial activity of the hybrid nanocomposite multifunctional coatings for possible applications in surgical equipment.

Acknowledgments

The authors gratefully acknowledge Dr. G. Sundararajan and Dr. G. Padmanabham for their keen support and constant encouragement provided throughout the course of this investigation. They also acknowledge Dr. Y.S. Rao for carrying out the Thermogravimetric analysis.

References

[1] S.M. Lee, B.S. Lee, T.G. Byun, K.C. Song, Preparation and antibacterial activity of silver-doped organic–inorganic hybrid coatings on glass substrates, Colloids and Surfaces A 355 (2010) 161–165.

[2] M. Mennig, M. Schmitt, H. Schmidt, Synthesis of Ag-colloids in sol–gel derived SiO_2-coatings on glass, Journal of Sol–Gel Science and Technology 8 (1997) 1035–1042.

[3] H.J. Jeon, S.C. Yi, S.G. Oh, Preparation and antibacterial effects of Ag-SiO_2 thin films by sol–gel method, Biomaterials 24 (2003) 4921–4928.

[4] M. Marini, D.D. Niederhausern, R. Iseppi, M. Bondi, C. Sabia, M. Toselli, F. Pilati, Antibacterial activity of plastics coated with silver-doped organic–inorganic hybrid coatings prepared by sol–gel processes, Biomacromolecules 8 (2007) 1246–1254.

[5] N. Lubick, Nanosilver toxicity: Ions, nanoparticles or both, Environmental Science & Technology 42 (2008) 8617.

[6] I. Perelshtein, G. Applerot, N. Perkas, E. Wehrschuetz-Sigl, A. Hasmann, G. Guebitz, A. Gedanken, CuO-cotton nanocomposite: formation, morphology and antibacterial activity, Surface & Coatings Technology 204 (2009) 54–57.

[7] J. Gabbay, G. Borkow, J. Mishal, E. Magen, R. Zatcoff, Y. Shemer-Avni, Copper oxide impregnated textiles with potential biocidal activities, Journal of Industrial Textiles 35 (2006) 323–335.

[8] G. Ren, D. Hub, E.W.C. Cheng, M.A. Vargas-Reus, P. Reip, R.P. Allaker, Characterization of copper oxide nanoparticles for antimicrobial applications, International Journal of Antimicrobial Agents 33 (2009) 587–590.

[9] O. Akhavan, E. Ghaderi, Cu and CuO nanoparticles immobilized by silica thin films as antibacterial materials and photocatalysts, Surface & Coatings Technology 205 (2010) 219–223.

[10] Q. Yu, X. Ma, M. Wang, C. Yu, T. Bai, Influence of embedded particles on microstructure, corrosion resistance and thermal conductivity of CuO/SiO_2 and NiO/SiO_2 nanocomposite coatings, Applied Surface Science 254 (2008) 5089–5094.

[11] I.B. Ditta, A. Steele, C. Liptrot, J. Tobin, H. Tyler, H.M. Yates, D.W. Sheel, H.A. Foster, Photocatalytic antimicrobial activities of thin surface films of TiO_2, CuO and TiO_2/CuO dual layers on *Escherichia coli* and bacteriophage T4, Applied Microbiology and Biotechnology 79 (2008) 127–133.

[12] G. Grundmeier, W. Schmidt, M. Stratmann, Corrosion protection by organic coatings: electrochemical mechanism and novel methods of investigation, Electrochimica Acta 45 (2000) 2515–2533.

[13] R. Haneda, K. Aramaki, Protective films on copper by multistep modification on an alkanethiol monolayer of chlorosilanes and alkanediol, Journal of the Electrochemical Society 145 (1998) 2786–2791.

[14] W. Lu, R.L. Elsenbaumer, T. Chen, V.G. Kulkarni, Corrosion protection of metals by conductive polymers III. Improved performance and inhibition in NaCl, Materials Research Society Symposium Proceedings 488 (1998) 653–658.

[15] D.C.L. Vasconcelos, J.A.N. Carvalho, M. Mantel, W.L. Vasconcelos, Corrosion resistance of stainless steel coated with sol–gel silica, Journal of Non-Crystalline Solids 273 (2000) 135–139.

[16] G. Ruhi, O.P. Modi, I.B. Singh, Pitting of AISI 304L stainless steel coated with nanostructured sol–gel alumina coatings in chloride containing acidic environments, Corrosion Science 51 (2009) 3057–3063.

[17] T.P. Chou, C. Chandrasekaran, G.Z. Cao, Sol–gel derived hybrid coatings for corrosion protection, Journal of Sol–Gel Science and Technology 26 (2003) 321–327.

[18] T.P. Chou, C. Chandrasekaran, S. Limmer, C. Nguyen, G.Z. Cao, Organic–inorganic sol–gel coating for corrosion protection of stainless steel, Journal of Materials Science Letters 21 (2002) 251–255.

[19] T.P. Chou, C. Chandrasekaran, S.J. Limmer, S. Seraji, Y. Wu, M.J. Forbess, C. Nguyen, G.Z. Cao, Organic–inorganic hybrid coatings for corrosion protection, Journal of Non-Crystalline Solids 290 (2001) 153–162.

[20] A. Pepe, M. Aparicio, A. Durán, S. Ceré, Cerium hybrid silica coatings on stainless steel AISI 304 substrate, Journal of Sol–Gel Science and Technology 39 (2006) 131–138.

[21] S. Ono, H. Tsuge, Y. Nishi, Improvement of corrosion resistance of metals by an environmentally friendly silica coating method, Journal of Sol–Gel Science and Technology 9 (2004) 147–153.

[22] M. Mennig, C. Schelle, A. Duran, J.J. Damborenea, M. Guglielmi, G. Brusatin, Investigation of glass-like sol–gel coatings for corrosion protection of stainless steel against liquid and gaseous attack, Journal of Sol–Gel Science and Technology 13 (1998) 717–722.

[23] D. Wang, G.P. Bierwagen, Sol–gel coatings on metals for corrosion protection, Progress in Organic Coatings 64 (2009) 327–338.
[24] C.J. Brinker, G.W. Scherer:, Sol–Gel Science: The Physics and Chemistry of Sol–Gel Processing, Academic Press, 1990,, p. 790.
[25] C.A. Schiller, W. Strunz, The evaluation of experimental dielectric data of barrier coatings by means of different models, Electrochimica Acta 46 (2001) 3619–3625.
[26] W.H. Mulder, J.H. Sluyters, T. Pajkossy, I. Nyikos, Tafel current at fractal electrodes: connection with admittance spectra, Journal of Electroanalytical Chemistry 285 (1990) 103–115.
[27] C.-H. Kim, S.-I. Pyun, J.-J. Kim, An investigation of the capacitance dispersion on the fractal carbon electrode with edge and basal orientations, Electrochimica Acta 48 (2003) 3455–3463.
[28] L. Feng, S. Li, Y. Li, H. Li, L. Zhang, J. Zhai, Y. Song, B. Liu, L. Zhiang, D. Zhu, Super-hydrophobic surfaces: from natural to artificial, Advanced Materials 14 (2002) 1857–1860.
[29] R.N. Wenzel, Resistance of solid surfaces to wetting by water, Industrial and Engineering Chemistry 28 (1936) 988–994.
[30] A.B.D. Cassie, S. Baxter, Wettability of porous surfaces, Transactions of the Faraday Society 40 (1944) 546–551.